AIP | The Journal of Chemical Physics

Maximum efficiency of state-space models of nanoscale energy conversion devices

Mario Einax and Abraham Nitzan

Citation: The Journal of Chemical Physics **145**, 014108 (2016); doi: 10.1063/1.4955160
View online: http://dx.doi.org/10.1063/1.4955160
View Table of Contents: http://scitation.aip.org/content/aip/journal/jcp/145/1?ver=pdfcov
Published by the AIP Publishing

Maximum efficiency of state-space models of nanoscale energy conversion devices

Mario Einax[a] and Abraham Nitzan
School of Chemistry, Tel Aviv University, Tel Aviv 69978, Israel

(Received 4 March 2016; accepted 22 June 2016; published online 6 July 2016)

The performance of nano-scale energy conversion devices is studied in the framework of state-space models where a device is described by a graph comprising states and transitions between them represented by nodes and links, respectively. Particular segments of this network represent input (driving) and output processes whose properly chosen flux ratio provides the energy conversion efficiency. Simple cyclical graphs yield Carnot efficiency for the maximum conversion yield. We give general proof that opening a link that separate between the two driving segments always leads to reduced efficiency. We illustrate these general result with simple models of a thermoelectric nanodevice and an organic photovoltaic cell. In the latter an intersecting link of the above type corresponds to non-radiative carriers recombination and the reduced maximum efficiency is manifested as a smaller open-circuit voltage. *Published by AIP Publishing.* [http://dx.doi.org/10.1063/1.4955160]

I. INTRODUCTION

Modeling of molecular scale engines such as photovoltaic cells, thermoelectric devices, light emitting diods and biological machines is often done in terms of a state-space description.[1] In such state-space models the processes underlying the device operation are described as transitions between microscopic system states, leading to the engine description in terms of a graph comprising nodes (=states) connected by bonds that represent transitions between them. On this network, the time evolution is determined by the rates associated with each bonds and fluxes associated with the non-equilibrium dynamics flow along interconnected linear and cyclical paths. Particular segments of this network represent the input (driving) and output (motion against load)[2] processes, where the corresponding rates deviate from restrictions imposed by equilibrium thermodynamics, thus maintaining the system in a non-equilibrium state. Such models usually constitute coarse grained descriptions of underlying detailed microscopic processes[3] that serve to simplify the theoretical and numerical analyses while maintaining focus on the significant parameters and time scales associated with the process under study. Similar models are often used to describe and analyze biochemical networks[4–6] and stochastic pumps.[7]

From the fundamental point of view, state-space models of nanoscale energy conversion devices are open systems that interact with an environment such that the energy and the number of particles can all vary subject to the constraints that their averaged values are fixed. To gain useful work by harvesting energy from fluctuating environments is the major challenge in the field of nanothermodynamics. To this end, a nanomachine should work against a load tending to reduce the current generated by driving force. The performance of such nanodevices strongly depends on the amount of energy and matter transferred across the boundary between the system's region and the environment. A thermodynamic analysis of nanoscale devices have found increasing attention in the scientific community.[8–13] It should be noted that without any driving and load we arrive at the standard equilibrium statistical mechanics of an open system.

Much progress has been made in the past understanding the efficiency and the efficiency at maximum power of state-space models of nanomachines.[14–21] Under finite power operation, the standard thermodynamic consideration of the entropy production in such systems is one way to describe the performance of energy-converting devices. Another quite illuminating concept is given by an elegant network representation[22] of the underlying master equation that allows one to decompose the stationary dynamics as cycles. In a seminal work, Seifert[23] showed that the efficiency at maximum power of autonomous (that is, steady state) nanomachines working under isothermal conditions can be studied within such cycle analysis framework. One main result of this work is that strongly coupled[24] multicycle machines obey the same relations for efficiency and efficiency at maximum power as unicyclic machines, while weakly coupled multicyclic machines found to be less efficient and their efficiency at maximum power is less universal even in the linear response regime. The present work extends some of these considerations to non-isothermal models needed for the analysis of molecular scale heat engines and reaches equivalent conclusions. Our analysis is done using, following Schnakenberg,[22] a convenient graph representation that relates the multi-cycle structure and its weak/strong coupling character to the graph topology.

Our goal here is to study the effect of intersecting pathways on the performance of nanoscale energy conversion devices that are simplistically described by a single cycle in state space. We give a general proof that opening a link that separate between the two driving segments (which are hence "weakly coupled") always leads to reduced

[a]Electronic mail: meinax@al.tau.ac.il

stopping (open circuit) and efficiency in autonomous non-isothermal nanomachines in contact with different heat reservoirs. To connect with realistic situation we point out that in applications to photoelectric devices such intersecting pathways correspond to carrier recombination. In addition, we discuss stopping condition for thermoelectric energy harvester as a further example.

II. MODELING DETAILS

Our discussion is based on the assumption that a suitable state space model can be constructed for the process of interest. Specifically, we require that (a) a coarse-grained description of the energy conversion processes in terms of system states and corresponding transition rates can be constructed, and (b) the input (driving) and output (flux against load) can be described in terms of transitions between these states. Thus, the starting point is a representation of the system dynamics by a kinetics scheme comprising systems states connected by (assumed known) rates, similar in spirit to transport theories based on lattice gas approaches[25–29] that find applications in other contexts, e.g., use of a master equation approach to analyze cell dynamics.[30–33] In the graph theory approach this kinetic scheme is represented by a graph that comprises nodes (corresponding to states) and edges (representing transitions between states), on which fluxes associated with the non-equilibrium dynamics flow along interconnected linear and cyclical paths. In this scheme, the observed macroscopic currents (average currents of macroscopic variables) through the systems, are linked through their circular counterparts to the microscopic transitions between individual states. Examples are shown in Fig. 1 that depicts single cycle models (henceforth referred to as model SC) for a photovoltaic cell [Figs. 1(a)-1(c)] or a thermoelectric device [Figs. 1(d) and 1(e)], both comprising N states that represent a charge carrier occupying different sites in the system and one state (denoted 0) in which the charge carrier is absent. Transition rates between system states $j = 0, 1, \ldots, N$ are determined by state energies E_j, the bias voltage V, and the local temperatures. The different rates satisfy detailed balance conditions,

$$\frac{k_{j+1,j}}{k_{j,j+1}} = e^{-\beta(E_{j+1}-E_j)} \tag{1}$$

($k_{i,j}$ is the rate coefficient for the $j \to i$ transition) for all j, $j+1$ except at the driving and load segments. For the photovoltaic model the rates at the latter segments satisfy

$$\frac{k_{s+1,s}}{k_{s,s+1}} = e^{-\beta_S(E_{s+1}-E_s)} \quad \text{(red segment)} \tag{2}$$

$$\frac{k_{1,0}}{k_{0,1}} = e^{-\beta(E_1-\mu_L)}, \; \frac{k_{N,0}}{k_{0,N}} = e^{-\beta(E_N-\mu_R)} \quad \text{(blue segment)}. \tag{3}$$

In the thermoelectric case the rates at the blue-red segment satisfy

$$\begin{aligned} \frac{k_{1,0}}{k_{0,1}} &= e^{-\beta_L(E_1-\mu_L)}, \\ \frac{k_{N,0}}{k_{0,N}} &= e^{-\beta_R(E_N-\mu_R)} \quad \text{(blue-red segment)}. \end{aligned} \tag{4}$$

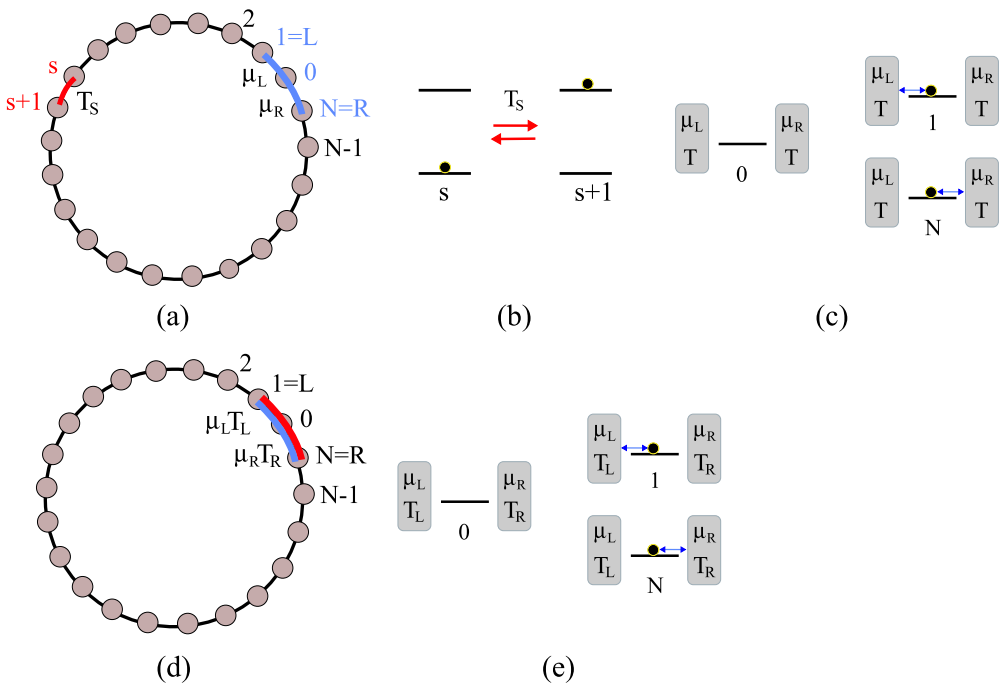

FIG. 1. (a) A simple graph (model SC) representing an ideal (no non-radiative losses) photovoltaic cell. The system is driven away from equilibrium by the processes that deposited at the red and blue segments. (b) Dynamics at the red segment: States s and $s+1$ are ground and excited states of a dye molecule and transition between them is driven by the "sun temperature" T_S. (c) Dynamics at the blue segment. The transitions $0 \rightleftharpoons 1$ and $0 \rightleftharpoons N$ represent changes in the number of electrons on the molecule due to its coupling to the left and right electrodes, respectively. Non-equilibrium is imposed by the different temperatures $T \neq T_S$ and by the voltage difference $V = \mu_R - \mu_L$ between the two electrodes (the electron charge e is set to 1 here and below). (d) Model SC for a simple thermoelectric device. Here the driving and load processes are positions at the same part of the cycle—between states $(1, 0)$ and $(0, N)$ that are characterized by different chemical potentials as well as different local temperatures (see panel (e).

Here, $\beta = (k_B T)^{-1}$, $\beta_K = (k_B T_K)^{-1}$, and $K = S, L, R$. The cycle affinity $\mathcal{A}$ is defined by[22]

$$\mathcal{A} = -\ln \mathcal{K}, \tag{5}$$

where $\mathcal{K}$ is the ratio between products of forward and backward rates

$$\mathcal{K} = \frac{k_{0,N} k_{N,N-1} \cdots k_{2,1} k_{1,0}}{k_{N,0} k_{N-1,N} \cdots k_{1,2} k_{0,1}}. \tag{6}$$

In the photovoltaic example, the stopping (open-circuit, OC) voltage is determined by the condition that the drivings associated with the voltage V and with the difference between T and T_S balance each other so that the steady state current through the system vanishes. In this case, the cycle affinity vanishes,[34] namely, $\mathcal{K} = 1$. Denoting the corresponding voltage $\mu_R - \mu_L$ by $V_{\rm OC}$ and using Eqs. (1)-(3) this leads to

$$\frac{V_{\rm OC}}{\Delta E} = 1 - \frac{T_{\rm low}}{T_{\rm high}} = 1 - \frac{T}{T_S} \equiv \eta_C, \tag{7}$$

with $T_{\rm low} = T$ and $T_{\rm high} = T_S$, and $\Delta E = E_{s+1} - E_s$. The l.h.s is $\lim_{J\to 0} \eta(J)$, where $\eta(J) = V(J)/\Delta E$ is the thermodynamic ("internal") efficiency of the device and J is the steady state current (same through all links). Equation (7) thus yields the Carnot expression η_C for the efficiency in the zero power limit. It also highlights the OC voltage as an important attribute in the quest to understand cell performance.[35–38] A similar result is obtained for the zero power limit of the thermoelectric device depicted in Figs. 1(d) and 1(e), provided that the ambient temperature T is taken the same as either T_L or T_R.[39,40] (The more general case where $T \neq T_L, T_R$ so that the system is driven by two temperature differences can be analyzed using the same kinetic framework, see Sec. IV for details.) Returning to the photovoltaic case, in Ref. 41 we have derived two important generalizations of this result: First, if the transition $s \rightleftharpoons s+1$ results from the combinations of radiative and non-radiative processes whose forward/backward ratios are determined by temperatures T_S and T, respectively, Eq. (7) is replaced by a similar expression in which T_S is substituted by an effective temperature $T_{\rm eff} = T_S\left(1 + \frac{k_B T}{\Delta E} \ln\left[\frac{1+\rho}{1+\rho\exp[-(\beta-\beta_S)\Delta E]}\right]\right)^{-1} \simeq T_S\left(1 + \frac{k_B T}{\Delta E}\ln[1+\rho]\right)^{-1}$, where $\rho = k^{\rm NR}_{s,s+1}/k^{\rm R}_{s,s+1}$ is the ratio between the non-radiative and radiative relaxation rates.[42] Second, if one of the cycle processes involves charge separation that comes at an energy cost (exciton binding energy) E_B, Eq. (7) is replaced by[34]

$$\frac{V_{\rm OC}}{\Delta E} = \eta_C - \frac{E_B}{\Delta E}. \tag{8}$$

The later situation characterizes the operation of organic photovoltaic cells.[43–45]

III. STOPPING CONDITION VS. INTERSECTION TOPOLOGY

Model SC and Eqs. (5)-(8) constitute a convenient framework for analyzing the stopping voltage of photovoltaic cells and thermoelectric devices (as well as the corresponding light emitting diode and cooling devices) and, as shown in Refs. 14, 34, 39, and 40, can be used as a starting point for studying optimal performance in finite power operations, provided that information on the system electronic structure and dynamics can be incorporated into such state-space model. However, such single cycle models are oversimplified; realistic state-space models contain intersecting pathways that make the analysis that leads to Eqs. (5)-(7) more involved. For example, in state-space models of photovoltaic cells such intersecting pathways represent non-radiative losses, e.g., electron-hole recombination processes[46] that are expected to reduce efficiency.

As graphical structures, such intersecting pathways divide the cycle of model SC into separate cycles (see Fig. 2), making it possible to have steady states in which the current in the power-extracting segment vanishes while internal currents exist elsewhere in the system. While intuitively we expect lower efficiencies in such situations, no general proof for this is available.

Here, we consider two generalizations of model SC shown in Fig. 2. In one [Fig. 2(a)], an intersecting pathway divides the system cycle into two subcycles without separating between the two driving segments. In the second [Fig. 2(b)], the driving segments are positioned on different cycles. We show that (a) intersecting pathways of the type shown in Fig. 2(a) do not affect the stopping voltage, hence their zero power operation is characterized by the Carnot efficiency. (b) Intersecting pathways of the type shown in Fig. 2(b) lead to zero power efficiency smaller that the Carnot value. For photovoltaic cells this is manifested by a lower stopping (open circuit) voltage.

We start with model SC and take note of the two sites, m and n, between which a new pathway will be

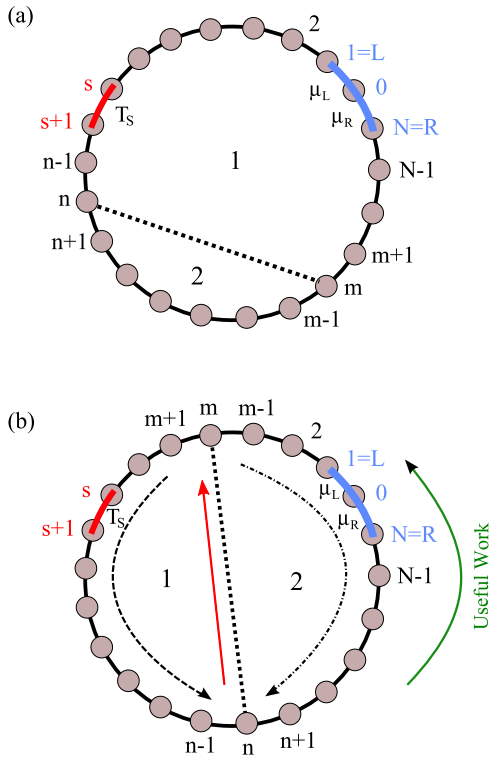

FIG. 2. Models characterized by intersected graphs—a new pathway is added between sites m and n. (a) The intersecting pathway does not separate the driving and load (red and blue) segments. (b) The bond n–m separates between the driving and load segments which now sit on different subcycles.

enabled. The rate ratio, Eq. (6), can obviously be written as $\mathcal{K} = \bar{\mathcal{K}}_1\bar{\mathcal{K}}_2$ where $\bar{\mathcal{K}}_1 = k_{n,n-1}\cdots k_{m+1,m}/k_{n-1,n}\cdots k_{m,m+1}$ and $\bar{\mathcal{K}}_2 = k_{m,m-1}\cdots k_{n+1,n}/k_{m-1,m}\cdots k_{n,n+1}$ are ratios of rate products that correspond to the arcs 1 and 2 in Fig. 2. Now enable the pathway between sites n and m, that is, make $k_{n,m}$ and $k_{m,n}$ different from zero. The graph is now divided into two subcycles, 1 and 2 in addition to the original cycle. The corresponding cycle rate-product ratios are

$$\mathcal{K}_1 = \bar{\mathcal{K}}_1\frac{k_{m,n}}{k_{n,m}}, \quad \mathcal{K}_2 = \bar{\mathcal{K}}_2\frac{k_{n,m}}{k_{m,n}} \tag{9}$$

so that $\mathcal{K}_1\mathcal{K}_2 = \bar{\mathcal{K}}_1\bar{\mathcal{K}}_2$.

Consider next the situation shown in Fig. 2(a), where the two driving segments are on the same subcycle 1. Starting from the model SC in the OC situation so that $\mathcal{K} = \mathcal{K}_1\mathcal{K}_2 = 1$, enabling the n–m link does not lead to current on this bond. To show this note that since all rates on arc 2 satisfy Eq. (1), we have $\bar{\mathcal{K}}_2 = e^{-\beta(E_m-E_n)} = k_{m,n}/k_{n,m}$. Equation (9) then yields $\mathcal{K}_2 = 1$ and therefore $\mathcal{K}_1 = 1$. Consequently, connecting the sites n and m will not create any extra current and subsequently does not affect the open-circuit voltage, hence the Carnot efficiency that characterizes this limit. Note that in thermoelectric devices depicted in Figs. 1(d) and 1(e) the cycle topology implies that intersecting pathways do not affect the device performance in the OC limit.[47]

In the situation of Fig. 2(b), each of the subcycles created by enabling the n–m pathway contains a non-equilibrium element, e.g., driving by the sun in subcycle 1 and the driving by the voltage in subcycle 2. Focusing on the latter and using Eqs. (1) and (3) yields

$$\bar{\mathcal{K}}_2 = e^{-\beta(E_m-E_n)}e^{-\beta\Delta\mu} = \frac{k_{m,n}}{k_{n,m}}e^{-\beta\Delta\mu}, \tag{10}$$

where $\Delta\mu = \mu_R - \mu_L$. Equation (9) then yields $\mathcal{K}_2 = \exp[-\beta\Delta\mu]$. This indicates that with the m–n link enabled the system cannot establish a state where currents through all links in subcycle 2 vanish unless $\Delta\mu = 0$.

To understand the consequence for the stopping voltage, let us set $k_{n,m} = \lambda\bar{k}_{n,m}$ and $k_{m,n} = \lambda\bar{k}_{m,n}$ and evaluate the derivative of this voltage, $V_{\rm OC}$, with respect to λ at $\lambda = 0$. $V_{\rm OC}$ is the value of $\Delta\mu = \mu_R - \mu_L$ for which the current between the electrodes, (the blue segment in Figs. 1 and 2), therefore across all links in arc 2, vanishes; namely $k_{j,j+1}P_{j+1} = k_{j+1,j}P_j$ for all these links. From Eqs. (1) and (3) it follows that when this current vanishes, the probabilities to find the system in states n and m are related to $V_{\rm OC}$ by

$$\frac{P_m}{P_n} = e^{-\beta(V_{\rm OC}+E_m-E_n)}. \tag{11}$$

It follows that

$$\left(\frac{dV_{\rm OC}}{d\lambda}\right)_{\lambda=0} = -c\left(\frac{d}{d\lambda}\frac{\bar{P}_m}{\bar{P}_n}\right)_{\lambda=0}, \tag{12}$$

where c is a positive number and $P_j = \bar{P}_j e^{-\beta E_j}$. The derivative on the r.h.s is negative if $(\bar{P}_m > \bar{P}_n)_{\lambda=0}$, i.e., $V_{\rm OC} < 0$, and negative in the opposite case $(\bar{P}_m < \bar{P}_n)_{\lambda=0}$; $V_{\rm OC} > 0$. This is a manifestation of the Le Chatelier's principle and can be inferred from the current expression, $J_{n\leftarrow m} = \lambda\left(\bar{k}_{n,m}P_m - \bar{k}_{m,n}P_n\right)$ by noting that

$$\left(\frac{dJ_{n\leftarrow m}}{d\lambda}\right)_{\lambda\to 0} = \left(\bar{k}_{n,m}P_m - \bar{k}_{m,n}P_n\right)_{\lambda=0} = \bar{k}_{n,m}e^{-\beta E_m}\left(\bar{P}_m - \bar{P}_n\right)_{\lambda=0}$$

namely the established current acts to reduce $\bar{P}_m/\bar{P}_n$ if it is larger, and increase it when it is smaller, than 1. Hence

$$\left(\frac{d|V_{\rm OC}|}{d\lambda}\right)_{\lambda=0} < 0. \tag{13}$$

Enabling the m–n link in the scheme of Fig. 2(b) thus results in reduction of the OC (stopping) voltage, namely, of the maximum thermodynamic efficiency,[48] as found in Ref. 23.

IV. EXAMPLES

As already noted, this general result can be applied to a wide range of nano-scale energy conversion devices like thermoelectric energy converter, heating engines or refrigerator, enzymatic networks, etc. To illustrate this general observation, we consider simple state-space models, which can represent an organic photovoltaic cell comprising a donor acceptor D-A complex placed between two electrodes[34,41,49] as well as other recently discussed devices,[50,51] thermophotovoltaic device setups,[52] or thermoelectric energy harvester.[10]

A. Organic photovoltaic cell

Let us consider state-space model for organic photovoltaic device setups which are formulated on the microscopic level by identifying relevant rate kinetic processes. First, we calculate the stopping voltage, $V_{\rm OC} = \Delta\mu_{\rm OC}/|e|$, of the model of Fig. 3 for which the underlying graph has the topology shown in Fig. 4. As already mentioned, such a graph topology can represent an organic photovoltaic cell comprising a donor (D) and an acceptor (A) species placed in an interpenetrating

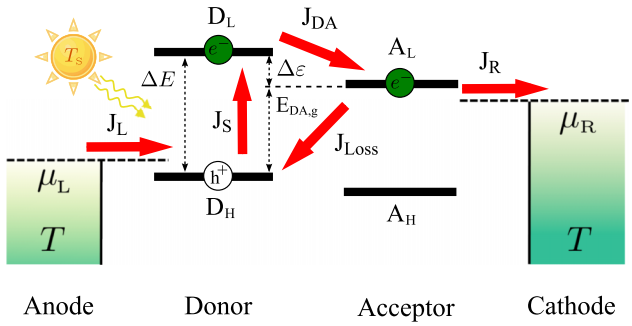

FIG. 3. A schematic representation of an organic photovoltaic cell. The system consists of a donor and acceptor, each characterized by their HOMO (D_H, A_H) and LUMO (D_L, A_L) levels. The energy spacing ΔE between the donor levels is the optical gap. The system is excited by solar energy (temperature T_S) across this gap, making it possible to drive current between the (biased) left and right electrodes. It is assumed that the D-phase is coupled only to the anode, while the A-phase is coupled only to the cathode. J_L (J_R) is the current entering (leaving) the solar system from (to) the electrodes, J_S is the light-induced transition current between the HOMO and the LUMO in the donor phase, and J_{DA} is the average current between the donor and acceptor species. J_{Loss} is the loss current which describes nonradiative recombination processes at the D-A interface.

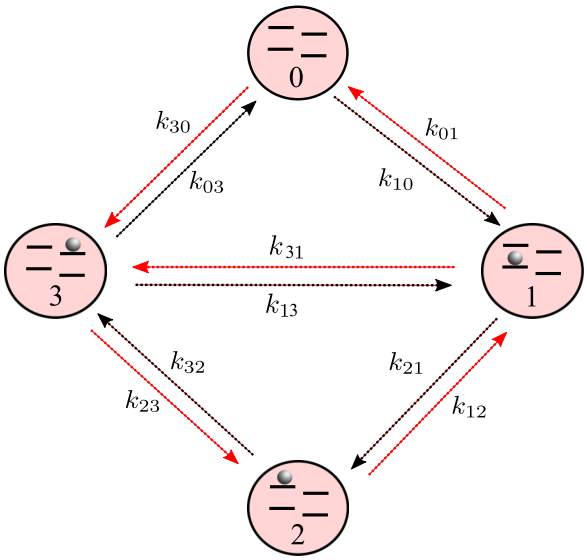

FIG. 4. A 4-level spinless model of an organic photovoltaic cell.[41,49] The states are: 0—no excess electron, 1—excess electron in the higher occupied molecular orbital (HOMO) of the donor, 2—Following an optical transition, electron is on the otherwise lower unoccupied molecular orbital (LUMO) of the donor (an exciton state). 3: Following charge separation, the electron has moved to the acceptor LUMO. The transitions $3 \rightleftharpoons 0$ and $0 \rightleftharpoons 1$ include electron transfer to the right and left electrode, respectively, $1 \rightleftharpoons 2$ is the optical excitation process and $2 \rightleftharpoons 3$ is the exciton dissociation process (see Ref. 41 for further details). The process $3 \rightleftharpoons 1$ that divides the cycle to two subcycles represents radiationless recombination.

architecture between two electrodes,[34,41,49] where the stopping voltage is generally referred to as the open-circuit voltage. For simplicity we limit ourselves to a four-state model that, despite its simplicity, can account for important interfacial electronic processes, including excitation, exciton dissociation, carrier recombination and electron transfer (ET) processes (see Fig. 3).

For this example, the D and A species are characterized by their molecular HOMO $(\varepsilon_{\mathrm{D_H}}, \varepsilon_{\mathrm{A_H}})$ and LUMO $(\varepsilon_{\mathrm{D_L}}, \varepsilon_{\mathrm{A_L}})$ levels (see Fig. 3). These translate into three relevant energy differences $\Delta E = \varepsilon_{\mathrm{D_L}} - \varepsilon_{\mathrm{D_H}}$ (the optical gap), $\Delta\epsilon = \varepsilon_{\mathrm{D_L}} - \varepsilon_{\mathrm{A_L}}$ (interfacial LUMO-LUMO gap), and $E_{DA,g} = \varepsilon_{\mathrm{A_L}} - \varepsilon_{\mathrm{D_H}}$ (effective band gap). The four states are enumerated according to the population on the levels (D_H, D_L, A_L, A_H): $0 = (0,0,0,1)$, $1 = (1,0,0,1)$, $2 = (0,1,0,1)$, $3 = (0,0,1,1)$ (the acceptor HOMO is always occupied). The corresponding probabilities P_0, P_1, P_2, and P_3 fulfil the normalization condition $\sum_{k=0}^{3} P_k = 1$. The system dynamics is modeled by a master equation approach accounting for the time evolution of the probabilities $P_j(t)$ with $j = 0,1,2,3$,

$$\frac{dP_0(t)}{dt} = k_{01}P_1(t) + k_{03}P_3(t) - (k_{10} + k_{30})\,P_0(t), \quad (14)$$

$$\frac{dP_1(t)}{dt} = k_{10}P_0(t) + k_{12}P_2(t) + k_{13}P_3 - (k_{01} + k_{21} + k_{31})\,P_1(t), \quad (15)$$

$$\frac{dP_2(t)}{dt} = k_{21}P_1(t) + k_{23}P_3(t) - (k_{12} + k_{32})\,P_2(t), \quad (16)$$

$$\frac{dP_3(t)}{dt} = k_{30}P_0(t) + k_{31}P_1(t) + k_{32}P_2(t) - (k_{03} + k_{23} + k_{13})\,P_3(t). \quad (17)$$

The processes $0 \leftrightarrow 1$ and $0 \leftrightarrow 3$ correspond to electron transfer between the left electrode and the donor level D_H and between the right electrode and the acceptor level A_L. The process $1 \leftrightarrow 2$ is the light induced transition at the donor and $2 \leftrightarrow 3$ corresponds to the exciton dissociation. Finally, the additional process (link between states 1 and 3) that intersects the graph in Fig. 4 represents non-radiative recombination. This loss process returns a free electron on the acceptor back to the donor ground state. The corresponding rates satisfy the detailed balance relations:

$$\frac{k_{10}}{k_{01}} = e^{-\beta(E_1-\mu_{\mathrm{L}})}, \quad \frac{k_{3,0}}{k_{0,3}} = e^{-\beta(E_3-\mu_{\mathrm{R}})}, \quad (18)$$

$$\frac{k_{21}}{k_{12}} = e^{-\beta_S \Delta E}, \quad (19)$$

$$\frac{k_{32}}{k_{23}} = e^{-\beta(E_3-E_2+E_B)}, \quad (20)$$

$$\frac{k_{13}}{k_{31}} = e^{-\beta(E_1-E_3)}, \quad (21)$$

where $E_1 = \varepsilon_{D_H}$, $E_2 = \varepsilon_{D_L}$, $E_3 = \varepsilon_{A_L}$, $\Delta E = E_2 - E_1$, and E_B is the exciton binding energy.

In the absence of the $1 \leftrightarrow 3$ process, that is, when $k_{31} = k_{13} = 0$ the open-circuit situation amounts to zero current through all links in the system. The corresponding equations

$$\begin{pmatrix} k_{10} & -k_{01} & 0 & 0 \\ -k_{30} & 0 & 0 & k_{03} \\ 0 & k_{21} & -k_{12} & 0 \\ 0 & 0 & k_{32} & -k_{23} \end{pmatrix} \begin{pmatrix} P_0 \\ P_1 \\ P_2 \\ P_3 \end{pmatrix} = 0 \quad (22)$$

implies that the determinant of the rate matrix in (23) vanishes. This yields

$$\frac{k_{10}k_{03}k_{32}k_{21}}{k_{01}k_{30}k_{12}k_{23}} = 1 \quad (23)$$

that using Eqs. (18)-(20) leads to

$$V_{\mathrm{OC}} = \Delta E \left(1 - \frac{T}{T_{\mathrm{S}}}\right) - E_{\mathrm{B}}. \quad (24)$$

The maximum thermodynamic efficiency is correspondingly $\eta_C - E_B/\Delta E$, highlighting the loss associated with the exciton binding energy.

When the process $3 \leftrightarrow 1$ is enabled, Eq. (22) is generalized to

$$\begin{pmatrix} k_{10} & -k_{01} & 0 & 0 \\ -k_{30} & 0 & 0 & k_{03} \\ 0 & k_{21}+k_{31} & -k_{12} & -k_{13} \\ 0 & k_{31} & k_{32} & -k_{23}-k_{13} \end{pmatrix} \begin{pmatrix} P_0 \\ P_1 \\ P_2 \\ P_3 \end{pmatrix} = 0. \quad (25)$$

The vanishing of the corresponding determinant now leads to

$$\frac{k_{10}k_{03}k_{32}k_{21}}{k_{01}k_{30}k_{12}k_{23}} = \frac{1 + k_{13}\frac{k_{12}+k_{32}}{k_{12}k_{23}}}{1 + k_{31}\frac{k_{12}+k_{32}}{k_{21}k_{32}}}. \quad (26)$$

That again using Eqs. (18)-(21) yields the following expression for the open-circuit voltage:

$$V_{\rm OC}(\lambda) = \Delta E\eta_C - E_B - k_BT \ln \frac{1 + k_{13}\dfrac{k_{12}+k_{32}}{k_{12}k_{23}}}{1 + k_{31}\dfrac{k_{12}+k_{32}}{k_{21}k_{32}}}, \tag{27}$$

setting $k_{13} = \lambda\bar{k}_{13}$ and $k_{31} = \lambda\bar{k}_{31}$ and taking the derivative with respect to λ we find, using also Eqs. (18)-(21)

$$\left(\frac{dV_{\rm OC}}{d\lambda}\right)_{\lambda=0} = -k_BT\frac{\bar{k}_{13}(k_{32}+k_{12})}{k_{12}k_{23}}\left(1 - e^{-\beta(V_{\rm OC})_{\lambda=0}}\right), \tag{28}$$

where $(V_{\rm OC})_{\lambda=0}$ is given by (8). This is an explicit statement of the inequality (13).

B. Thermoelectric energy harvester

Now, we consider a simple state-space model for one-dimensional thermoelectric nanosystems comprising N states that represent a charge carrier occupying different sites in the system and one state (denoted 0) in which the charge carrier is absent. Transition rates between system states $j = 0, 1, \ldots, N$ are determined by state energies E_j, the bias voltage $\Delta\mu = \mu_L - \mu_R = V$, and the local temperatures T_L, T_R, and T. For example, $T_L > T \geq T_R$. Following the explanation in the main text, steady state dynamics can be represented by a graph similar to Fig. 1. The dynamics at the segments between states 1 and N are dictated by the energy reservoir at temperature T, while the transition between state 0 and 1 is driven by the energy reservoir at temperature T_L, and the transition between state N and 0 is driven by the energy reservoir at temperature T_R. The transitions $0 \rightleftharpoons 1$ and $0 \rightleftharpoons N$ also include the particle exchange of the system with the environment. The corresponding rates satisfy the detailed balance relations,

$$\frac{k_{1,0}}{k_{0,1}} = e^{-\beta_{\rm L}(E_1-\mu_{\rm L})}, \qquad \frac{k_{N,0}}{k_{0,N}} = e^{-\beta_R(E_N-\mu_{\rm R})}, \tag{29}$$

$$\frac{k_{2,1}}{k_{1,2}} = e^{-\beta(E_2-E_1)}, \tag{30}$$

$$\frac{k_{N,N-1}}{k_{N-1,N}} = e^{-\beta(E_N-E_{N-1})}, \tag{31}$$

where $\beta_R^{-1} = k_BT_R$, $\beta_L^{-1} = k_{\rm B}T_L$, and $\beta^{-1} = k_{\rm B}T$.

At a particular value, $V_{\rm OC}$, the charge current stops. This stopping voltage can be obtained by looking at the ratio between products of forward and backward rates of the underlying cycle graph

$$\begin{aligned}\mathcal{K} &= \frac{k_{0,N}k_{N,N-1}\cdots k_{2,1}k_{1,0}}{k_{N,0}k_{N-1,N}\cdots k_{1,2}k_{0,1}},\\ &= e^{\beta_R(E_N-\mu_R)}e^{\beta(E_N-E_{N-1})}\\ &\quad \cdots e^{-\beta(E_2-E_1)}e^{-\beta_L(E_1-\mu_L)},\\ \mathcal{K} &= e^{\beta_R(E_N-\mu_R)-\beta(E_N-E_1)-\beta_L(E_1-\mu_L)} \equiv e^{-\mathcal{A}}.\end{aligned} \tag{32}$$

Setting $\mathcal{A} = 0$, we arrive at the stopping condition

$$\beta_R\mu_R - \beta_L\mu_L = E_N(\beta_R - \beta) - E_1(\beta_L - \beta), \tag{33}$$

where the electrical current driven by heat flows vanishes. If $E_1 = E_N$, the stopping condition (33) reduces to $\beta_R\mu_R - \beta_L\mu_L = E_1(\beta_R - \beta_L)$, which depends only on the temperatures T_L and T_R.

In particular, we consider two different types in applying the voltage drops between the systems and the contacts, which leads to different values $V_{\rm OC}$. First, we consider that $\Delta\mu = \mu_R - \mu_L = V_{\rm OC}$. By setting $\mu_L = \varepsilon_F$, Eq. (33) leads to the stopping voltage

$$V_{\rm OC} = E_N\frac{(\beta_R - \beta)}{\beta_R} - E_1\frac{(\beta_L - \beta)}{\beta_R} - \varepsilon_F(1 - \frac{\beta_L}{\beta_R}). \tag{34}$$

If $E_N = E_1$, we have $V_{\rm OC} = (E_1 - \varepsilon_F)(1 - \frac{\beta_L}{\beta_R})$. As a second case, we choose chemical potentials of the contacts, which are symmetrically, i.e., $\mu_L = \varepsilon_L - V_{\rm OC}/2$ and $\mu_R = \varepsilon_L + V_{\rm OC}/2$. Then, we obtain for the stopping voltage the following expression:

$$V_{\rm OC} = 2\left[E_N\frac{(\beta_R - \beta)}{\beta_R + \beta_L} - E_1\frac{(\beta_L - \beta)}{\beta_R + \beta_L} - \varepsilon_F(\frac{\beta_{\rm R} - \beta_L}{\beta_R + \beta_L})\right]. \tag{35}$$

If $E_N = E_1$, we have $V_{\rm OC} = 2(E_1 - \varepsilon_F)(\frac{\beta_R - \beta_L}{\beta_R + \beta_L})$. Finally, we discuss the special choice $\varepsilon_F = (E_N + E_1)/2$ and $E_N \neq E_1$ according to Ref. 40. Thus, Eq. (34) can be written as

$$\begin{aligned}V_{\rm OC} &= (E_N - E_1)\left[1 - \frac{2\beta}{\beta_L + \beta_R}\right],\\ &\equiv (E_N - E_1)\left[1 - \frac{2}{T(T_L^{-1} + T_R^{-1})}\right],\end{aligned} \tag{36}$$

which can be seen as a generalization of Eq. (7) in the main text to three heat reservoirs when having one effective energy gap in the system under consideration. In particular, if T is equal to either T_L or T_R we get the Carnot efficiency as mentioned in the main text. Differently speaking, the stopping (OC) voltage is dictated by the effective energy gap $\Delta E = \varepsilon_n - \varepsilon_1$ between site n and site 1 and generally depends on three temperature T_L,T_R, and T. It is also interesting to note that if we choose $T_L = T_R < T$ in Eq. (36) we have no longer a thermoelectric nanomachine and switch to a nanoscale heat engine.

The analysis of loss processes can be done analogously to the first example given by an organic photovoltaic device setup (see Sec. IV A). To this end we will analyze a four state-space model given in Fig. 5. The four states are enumerated according to the population on the levels (n_1, n_2, n_3):

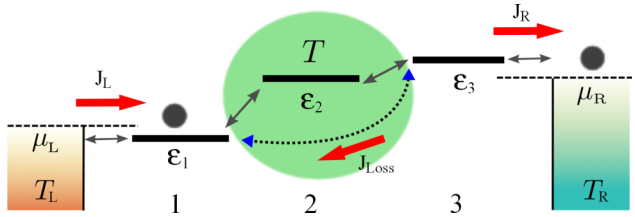

FIG. 5. Artificial (simple) thermoelectric nanojunction consisting of 3 sites and a given energy landscape characterized by the site energy levels ε_k; $k = 1, \ldots, 3$. The sites 1 and 3 are coupled to two particle reservoirs with chemical potentials μ_L and μ_R, respectively. Particles are injected or ejected from the two reservoir sites with rates that fulfil the condition of detailed balance with respect to the grand-canonical ensembles associated with μ_L and μ_R [see Eq. (29)]. In addition, the left lead L is coupled to an energy reservoir at temperature T_L and the right lead R is coupled to an energy reservoir T_R, while the junction between site 1 and site 3 is coupled to an energy reservoir at temperature T.

0 = (0,0,0), 1 = (1,0,0), 2 = (0,1,0), 3 = (0,0,1). Then, the corresponding rate processes can also be described by Eqs. (14)-(17). The processes $0 \leftrightarrow 1$ and $0 \leftrightarrow 3$ correspond to electron transfer between the left electrode and the level 1 and between the right electrode and the level 3. The processes $1 \leftrightarrow 2$ and $2 \leftrightarrow 3$ are phonon-assisted hopping processes due to the coupling to a phonon bath at temperature T. Finally, the additional process (link between states 1 and 3) that intersect the graph in Fig. 4 represent a loss channel. This loss process returns an electron from site 3 back to site 1. The open-circuit situation can be studied by repeating the analysis presented in the Sec. IV A. Again, we have to solve Eq. (25) and arrive at

$$\beta_R\mu_R - \beta_L\mu_L = E_3(\beta_R - \beta) - E_1(\beta_L - \beta) - \ln\frac{1 + k_{13}\dfrac{k_{12}+k_{32}}{k_{12}k_{23}}}{1 + k_{31}\dfrac{k_{12}+k_{32}}{k_{21}k_{32}}}. \quad (37)$$

In particular, for the case $\mu_L = \varepsilon_L - V_{OC}/2$ and $\mu_R = \varepsilon_L + V_{OC}/2$ we find for the stopping voltage

$$V_{OC} = 2\left[E_3\frac{(\beta_R - \beta)}{\beta_R + \beta_L} - E_1\frac{(\beta_L - \beta)}{\beta_R + \beta_L} - \varepsilon_F\left(\frac{\beta_R - \beta_L}{\beta_R + \beta_L}\right)\right] - \frac{2}{\beta_R + \beta_L}\ln\frac{1 + k_{13}\dfrac{k_{12}+k_{32}}{k_{12}k_{23}}}{1 + k_{31}\dfrac{k_{12}+k_{32}}{k_{21}k_{32}}}. \quad (38)$$

Note that this expression can also be used in the limit $k_{31} = 0$, i.e., $k_{31} \ll k_{13}$.

V. CONCLUSIONS

In conclusion, we have analyzed the performance of state-space network models of nanoscale energy conversion devices, focusing on their maximum efficiency (zero power) operation. A general argument based on cycle analysis yields conditions under which the opening of intersecting pathways in an otherwise cyclical graph leads to a decrease in the maximum efficiency. In the application to the operation of a photovoltaic cell such intersecting link often corresponds to a carrier recombination process, and its consequence is manifested in a reduced stopping (OC) voltage. It should be emphasized that similar analysis can be carried out for more complex models that include, for example, polaron formation and hot exciton dissociation, provided that they can be modeled by kinetic transitions in the system state-space. Finally, as described elsewhere,[34] such an approach can be used for analysis of optimal performance under finite power operation, although with the unavoidable loss of the generality associated with a thermodynamic description.

[1]U. Seifert, Rep. Prog. Phys. **75**, 126001 (2012).

[2]"Driving" and "load" should be understood in a general sense. Moving against a load can be moving against a potential bias and also transferring heat from a cold to a hot reservoir. Depending on the engine, the designation of processes as "driving" and "moving against a load" can interchange.

[3]H. van Eersel, R. A. J. Janssen, and M. Kemerink, Adv. Funct. Mater. **22**, 2700 (2012).

[4]T. L. Hill, J. Theor. Biol. **10**, 442 (1966).

[5]T. L. Hill, *Free Energy Transduction and Biochemical Cycle Kinetics*, 2nd ed. (Dover, New York, 2009).

[6]E. Gerritsma and P. Gaspard, Biophys. Rev. Lett. **05**, 163 (2010).

[7]S. Rahav, J. Horowitz, and C. Jarzynski, Phys. Rev. Lett. **101**, 140602 (2008).

[8]B. Rutten, M. Esposito, and B. Cleuren, Phys. Rev. B **80**, 235122 (2009).

[9]M. Esposito, K. Lindenberg, and C. V. den Broeck, Europhys. Lett. **85**, 60010 (2009).

[10]J.-H. Jiang, O. Entin-Wohlman, and Y. Imry, Phys. Rev. B **85**, 075412 (2012).

[11]J. Rossnagel, O. Abah, F. Schmidt-Kaler, K. Singer, and E. Lutz, Phys. Rev. Lett. **112**, 030602 (2014).

[12]Y. Zang, C. Huang, J. Wang, G. Lin, and J. Chen, Energy **85**, 200 (2015).

[13]O. Entin-Wohlman, Y. Imry, and A. Aharony, Phys. Rev. B **91**, 054302 (2015).

[14]M. Esposito, K. Lindenberg, and C. Van den Broeck, Phys. Rev. Lett. **102**, 130602 (2009).

[15]M. Esposito, R. Kawai, K. Lindenberg, and C. Van den Broeck, Phys. Rev. Lett. **105**, 150603 (2010).

[16]B. Gaveau, M. Moreau, and L. S. Schulman, Phys. Rev. Lett. **105**, 060601 (2010).

[17]G. Benenti, K. Saito, and G. Casati, Phys. Rev. Lett. **106**, 230602 (2011).

[18]Y. Apertet, H. Ouerdane, C. Goupil, and P. Lecoeur, Phys. Rev. E **85**, 041144 (2012).

[19]A. E. Allahverdyan, K. V. Hovhannisyan, A. V. Melkikh, and S. G. Gevorkian, Phys. Rev. Lett. **111**, 050601 (2013).

[20]H. Hooyberghs, B. Cleuren, A. Salazar, J. O. Indekeu, and C. Van den Broeck, J. Chem. Phys. **139**, 134111 (2013).

[21]Y. Izumida and K. Okuda, Phys. Rev. Lett. **112**, 180603 (2014).

[22]J. Schnakenberg, Rev. Mod. Phys. **48**, 571 (1976).

[23]U. Seifert, Phys. Rev. Lett. **106**, 020601 (2011).

[24]The term "strongly coupled" as referred to in Ref. 23 implies that the driving and load segments are positioned on the same (or very close) segment.

[25]M. Einax, G. C. Solomon, W. Dieterich, and A. Nitzan, J. Chem. Phys. **133**, 054102 (2010).

[26]M. Einax, M. Körner, P. Maass, and A. Nitzan, Phys. Chem. Chem. Phys. **12**, 645 (2010).

[27]M. Einax and P. Maass, Phys. Rev. E **80**, 020101(R) (2009).

[28]M. Dierl, P. Maass, and M. Einax, Europhys. Lett. **93**, 50003 (2011).

[29]M. Dierl, P. Maass, and M. Einax, Phys. Rev. Lett. **108**, 060603 (2012).

[30]A. Wagenpfahl, C. Deibel, and V. Dyakonov, IEEE J. Sel. Top. Quantum Electron. **16**, 1759 (2010).

[31]K. O. Sylvester-Hvid, S. Rettrup, and M. A. Ratner, J. Chem. B **108**, 4296 (2004).

[32]V. M. Burlakov, K. Kawata, H. E. Assender, G. A. D. Briggs, A. Ruseckas, and I. D. W. Samuel, Phys. Rev. B **72**, 075206 (2005).

[33]V. Rühle, A. Lukyanov, F. May, M. Schrader, T. Vehoff, J. Kirkpatrick, B. Baumeier, and D. Andrienko, J. Chem. Theory Comput. **7**, 3335 (2011).

[34]M. Einax and A. Nitzan, J. Phys. Chem. C **118**, 27226 (2014).

[35]K. Vandewal, K. Tvingstedt, A. Gadisa, O. Inganas, and J. V. Manca, Nat. Mater. **8**, 904 (2009).

[36]T. Kirchartz, K. Taretto, and U. Rau, J. Phys. Chem. C **113**, 17958 (2009).

[37]W. J. Potscavage, A. Sharma, and B. Kippelen, Acc. Chem. Res. **42**, 1758 (2009).

[38]P. K. Nayak, J. Bisquert, and D. Cahen, Adv. Mater. **23**, 2870 (2011).

[39]R. Sánchez and M. Büttiker, Phys. Rev. B **83**, 085428 (2011).

[40]A. N. Jordan, B. Sothmann, R. Sánchez, and M. Büttiker, Phys. Rev. B **87**, 075312 (2013).

[41]M. Einax, M. Dierl, and A. Nitzan, J. Phys. Chem. C **115**, 21396 (2011).

[42]This result is obtained from Eq. (26) of Ref. 34 by using the detailed balance relationships between the different rates.

[43]N. C. Giebink, G. P. Wiederrecht, M. R. Wasielewski, and S. R. Forrest, Phys. Rev. B **83**, 195326 (2011).

[44]L. J. A. Koster, S. E. Shaheen, and J. C. Hummelen, Adv. Energy Mater. **2**, 1246 (2012).

[45]M. Gruber, J. Wagner, K. Klein, U. Hörmann, A. Opitz, M. Stutzmann, and W. Brütting, Adv. Energy Mater. **2**, 1100 (2012).

[46]For example, the simplest representation of an organic photovoltaic cell the cycle undergone by the system is D_0A_0--(L) $\dashrightarrow$ D_1A_0 $\dashrightarrow$ $D_1^\star A_0$ $\dashrightarrow$ D_0A_1--(R) $\dashrightarrow$ D_0A_0. Here D and A are donor and acceptor, respectively and the subscript 0, 1 correspond to their electronic occupation. --(L) $\dashrightarrow$ represents a process where the system receives an electron from the left electrode and --(R) $\dashrightarrow$ is a process in which the system gives an electron to the right electrode. The process $D_0A_1 \dashrightarrow D_1A_0$ is a charge recombination process, which is an intersecting path of the type shown in Fig. 2(b). It is identical to the process represented by the 1–3 link in Fig. 4.

[47]Note, however, that we are considering a simple thermoelectric device model characterized by strong coupling (electrical current proportional to heat current[14]). More general situations may require further considerations.

[48]This assumes that all useful work is extracted at voltage-loaded segment and that the additional link is just another route by which the system tries to adjust to the imposed driving. Theoretically one could envision a device built with an additional load on this newly opened link that extracts additional useful work, thus moving the overall efficiency to a higher value. Our discussion disregards such scenario.

[49]M. Einax, M. Dierl, P. R. Schiff, and A. Nitzan, Europhys. Lett. **104**, 40002 (2013).

[50]A. Smirnov, L. Mourokh, P. Ghosh, and F. Nori, J. Phys. Chem. C **113**, 21218 (2009).

[51]F. Domínguez, S. Kohler, and G. Platero, Phys. Rev. B **83**, 235319 (2011).

[52]A. Lenert, D. M. Bierman, Y. Nam, W. R. Chan, I. Celanovic, M. Soljacic, and E. M. Wang, Nat. Nanotechnol. **9**, 126 (2014).